Polymer-Grafted Cellulose Fibers. II. Polymer Localization and Induced Alterations in Fiber Morphology

R. R. WARNER, E. REZAI*

Miami Valley Laboratories, P.O. Box 538707, Procter & Gamble Co., Cincinnati, Ohio 45253

Received 26 July 1996; accepted 17 January 1997

ABSTRACT: In methyl acrylate- or acrylonitrile-grafted northern softwood Kraft or southern softwood Kraft pulp fibers, polymer grafts are present almost homogeneously throughout the fiber wall, although some surface enhancement is observed. On unhydrolyzed fiber surfaces, acrylonitrile grafts protrude in clumps of tangled polymer tufts whereas methyl acrylate grafts form a more uniform, sometimes knobby surface coating. Grafting followed by hydrolysis causes extensive lengthwise splits in the S1 layer, which pulls away from the S2 layer. In the hydrolyzed solvent-dried fiber, the internal grafted polymer/cellulose domains create a unique filamentous and lamellar periodic substructure in the S2 wall. Coexisting with this substructure are numerous microvoids and occasional large pores. We believe that the enhanced absorbency of these fibers can be attributed to the S1 layer disruption, the presence of osmotically active polymer (sodium polyacrylate) incorporated extensively within the S2 wall, and the presence of a drastically altered, more accessible S2 wall substructure. Analytical electron microscopy is shown to be a useful technique for investigating polymer grafts in cellulose fibers. © 1997 John Wiley & Sons, Inc. J Appl Polym Sci **65:** 1471–1485, 1997

Key words: wood fiber; methyl acrylate; acrylonitrile; morphology; graft localization; electron microscopy; analytical electron microscopy; transmission electron microscopy; scanning electron microscopy

INTRODUCTION

As shown in our preceding article,[1] northern or southern softwood Kraft fibers grafted with acrylonitrile or methyl acrylate monomer followed by sodium hydroxide hydrolysis have a dramatically enhanced absorbency, and handsheets incorporating these fibers have increased absorbent capacity and rate of water absorption. It is known that enhanced absorbency can be attributed to changes in the driving forces for water uptake as well as changes in the inherent capillarity of the absorbing structure.[2] The fiber void structure determines the absorbent behavior of the fibers. In normal dried pulp fibers, microcapillaries exist in the form of slender, extremely small cavities.[3–5] The fibers are essentially nonporous.[5] Fibers dried from solvents are much more porous, with nearly a 2 order of magnitude increase in void volume such that microcapillaries are about 3.5 nm wide.[5] Refining and beating can further increase the void size by another order of magnitude.[6,7] To better understand the enhanced absorbency of our polymer-grafted cellulose fibers, we used microscopy to investigate both the location of polymer grafts on and within the fibers and the alterations in fiber morphology induced by the grafting process.

A relatively small number of techniques have been used to investigate the distribution of grafted polymers in cellulose fibers. Whereas techniques

Correspondence to: Dr. R. R. Warner.
* *Present Address:* Procter & Gamble Far East, Inc., Kobe Technical Center, 17-Koyo-cho Naka 1-chome, Higashinaduku, Kobe 658, Japan.

like infrared spectroscopy and scanning electron microscopy (SEM) are used to investigate surface grafting,[8–10] investigations of internal (volumetric) grafting have often relied on unsophisticated approaches. Simple inferences from physical parameters (sorption data, density[11]) or inferences from SEM observations[12,13] have been used to support internal grafting. More convincing studies used light microscopy to visualize uniformity of dye uptake as an indicator of grafted polymer distributions.[9,14,15] Because the resolution of light microscopy is very limited, transmission electron microscopy (TEM) has been used to visualize the distribution of polymer grafts within regions of the fiber wall[9,16–19] (for review, see Hebeish and Guthrie[20]). Although compelling, these latter studies nevertheless rely on multiple dissolution and washing steps that limit morphological resolution, potentially create artifacts, and are by nature an indirect determination of the polymer distribution. Finally, electron probe analysis has occasionally been used to indicate the distribution of grafts within polymer films[8,21,22] and the distribution of grafts and additives in paper[23] and fabric.[24,25]

Surprisingly, analytical electron microscopy (AEM) has apparently not been used to localize grafts in cellulose fibers. AEM has the ability to obtain high resolution morphological images and to correlate the morphological images with chemical element distributions. If the polymer intrinsically contains an element distinguishable from those of cellulose, such as nitrogen, then polymer localization is direct. Alternatively, if the polymer has chemical attributes different from those of cellulose, such as the presence of charged carboxylate groups, then unique inorganic counterions can be used to localize the polymer. Both of these approaches were used to investigate the distribution of acrylonitrile and acrylate polymer grafts within cellulose fibers. Light microscopy, SEM, microprobe analysis, and energy-filtered TEM were also used to investigate graft-induced alterations in fiber morphology.

EXPERIMENTAL

Fibers were grafted with acrylonitrile or methyl acrylate as described in the preceding article.[1] We analyzed hydrolyzed and unhydrolyzed fibers dried from ethanol. The grafting level in methyl acrylate fibers varied from 1 : 1 to 4 : 1 acrylate/fiber by weight[1]; typically the grafting level of analyzed fibers was 3 : 1.

Light Microscopy (LM)

A Wild stereomicroscope was used to photograph polymer-grafted fibers dispersed in water. Fiber visualization was enhanced by the addition of the histochemical stain toluidine-blue.

SEM

Fibers were secured to specimen stubs with double-sided Scotch tape. Analyses were performed with a Hitachi S-800 operated at 2 kV on uncoated or gold-palladium coated specimens.

TEM

Fiber specimens were submerged in nitrogen-free, preevacuated L. R. White resin (a polyhydroxylated aromatic acrylic resin for TEM embedment; Ted Pella Co., Redding, CA) and polymerized overnight at 60°C. Thin (80 nm) sections of ungrafted fibers were cut onto water using a Sorval MT2B ultramicrotome, picked up on bare EM grids, and stained with uranyl acetate and lead citrate following conventional procedures.[26] Thick (1 μm) sections of grafted and ungrafted fibers were cut dry using glass knives and were mounted dry on Formvar films stretched across nickel slot EM grids (Ted Pella Co.). The thick sections of fibers were analyzed unstained. TEM analyses were performed with a Zeiss EM902 operated at 80 kV using energy filtering to select zero-loss electrons.

AEM and Electron Microprobe Analysis

Both grafted and ungrafted fibers were embedded in L. R. White resin and 1-μm-thick sections were cut dry as described for TEM. Contrast-enhancing stains were not used. Analyses were performed with a Hitachi H-500 operated in the scanning TEM (STEM) mode at 100 kV and 0.5 nA sample current. Digital images and X-ray elemental analyses were obtained with a Tracor Northern 5500 energy dispersive spectrometer (EDS) equipped with a beryllium window (Noran Instruments, Madison, WI). With this system only elements of atomic number 11 (Na) and above can be detected. X-ray elemental maps were acquired for 4–8 h. X-ray elemental line scans were acquired

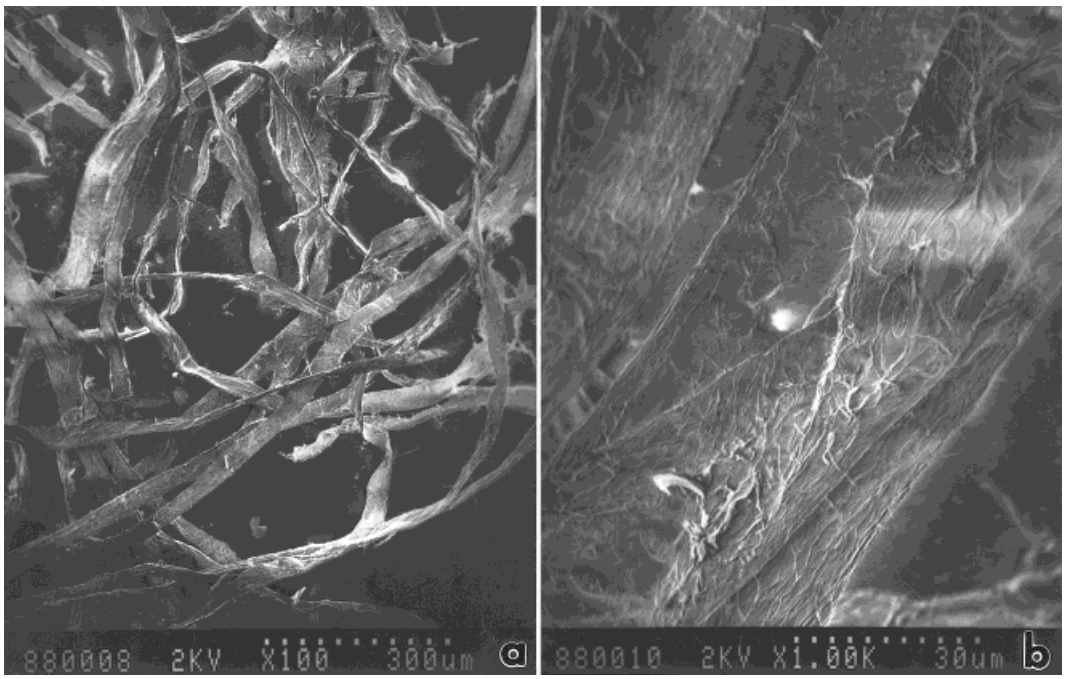

Figure 1 Control, ungrafted northern softwood Kraft (NSK) fibers. (a) SEM image; 100× original magnification. (b) Higher magnification SEM image; 1000× original magnification.

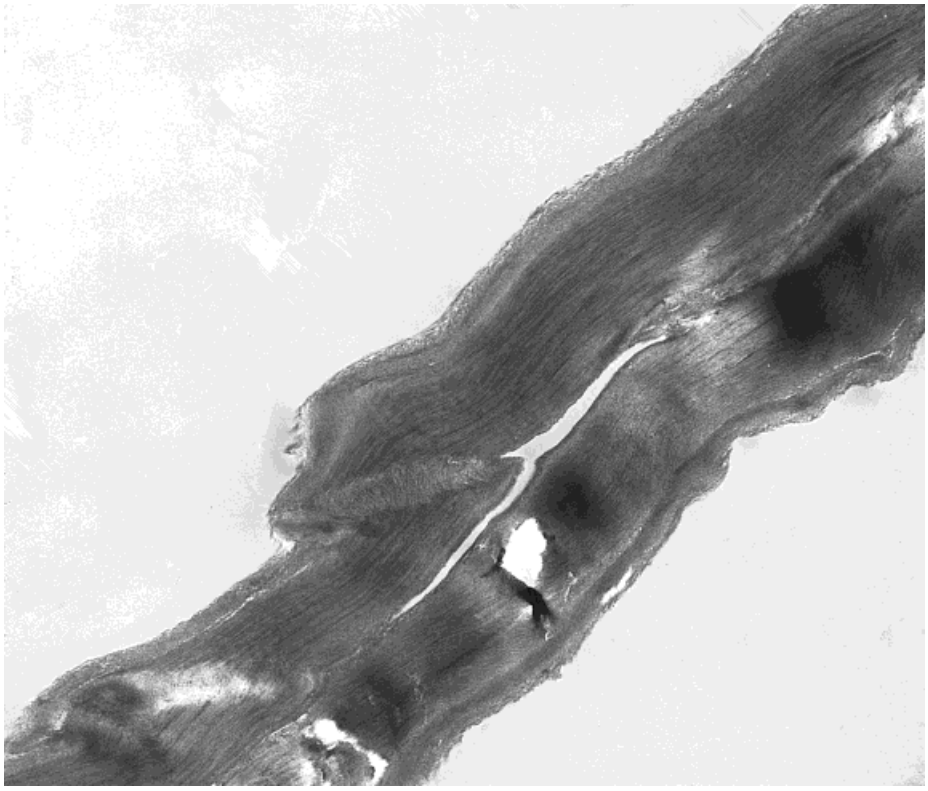

Figure 2 TEM image of a thin-sectioned, heavy metal stained ungrafted NSK fiber; 10,000× original magnification.

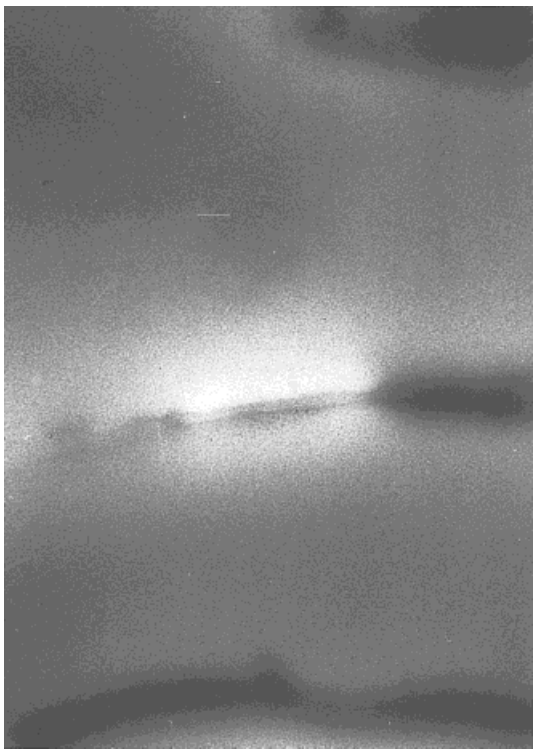

Figure 3 TEM image from a 1-μm-thick section of an unstained, ungrafted NSK fiber; 20,000× original magnification.

for times varying from several minutes to several hours. For nitrogen detection, sections were placed on Formvar-covered nickel slot grids that had been coated with evaporated aluminum in a vacuum evaporator. Analysis was with a Cameca MBX microprobe operated in the STEM mode at 10 kV and 20 nA sample current. Nitrogen detection utilized wavelength dispersive spectrometry with a lead stearate crystal. "Semiquantitative" nitrogen analyses were obtained with the Cameca TASK quantitative ZAF program using a bulk boron nitride standard.

Visualizing Carboxylate Groups by "Tagging" with Metal Ions

A technique originally described for localizing poly(acrylic acid) grafts in polyethylene films[21] was modified to allow carboxylate-containing polymer graphs to be distinguished from the cellulose matrix. Two methods were developed:

Method 1

Initially an ion exchange procedure was used to replace grafted acid functionalities with a unique metal salt (cesium) that could be detected by AEM. Grafted, hydrolyzed fibers were submerged under 0.1*N* HCl in a container blanketed with nitrogen gas. After 30 min the sample was filtered until dry, then covered with carbon dioxide free deionized distilled water. Using a pH titration system, the sample was titrated to pH 9 using cesium hydroxide. The sample was mechanically stirred and blanketed with nitrogen during this 6-h procedure. The sample was filtered, submerged under ethanol blanketed with nitrogen for an hour, and then filtered until dry.

Method 2

Following the hydrolysis step described in the article,[1] the sample was simply exhaustively washed overnight with deionized water to remove excess reagent (sodium hydroxide).

Chemical Measurements

Cesium Assay

Following the ion exchange, grafted fibers were ashed at 400°C in a muffle furnace for 3 h. The ash

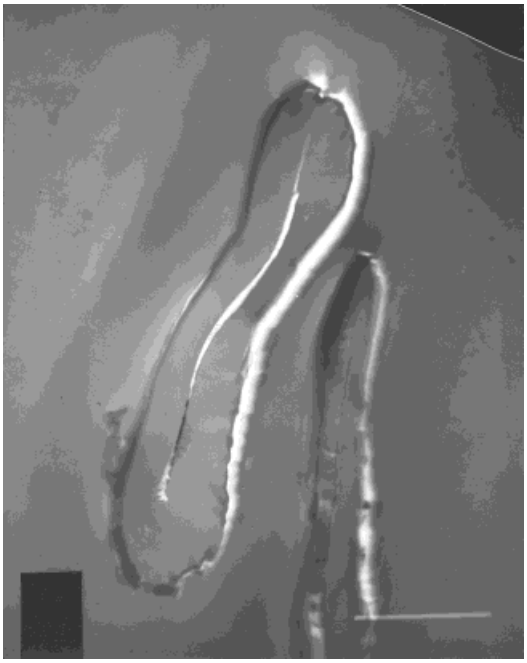

Figure 4 STEM image from a 1-μm-thick section of an unstained, ungrafted NSK fiber. The plastic/fiber junction often tears somewhat during sectioning; the tear is white in the image; 7500× original magnification.

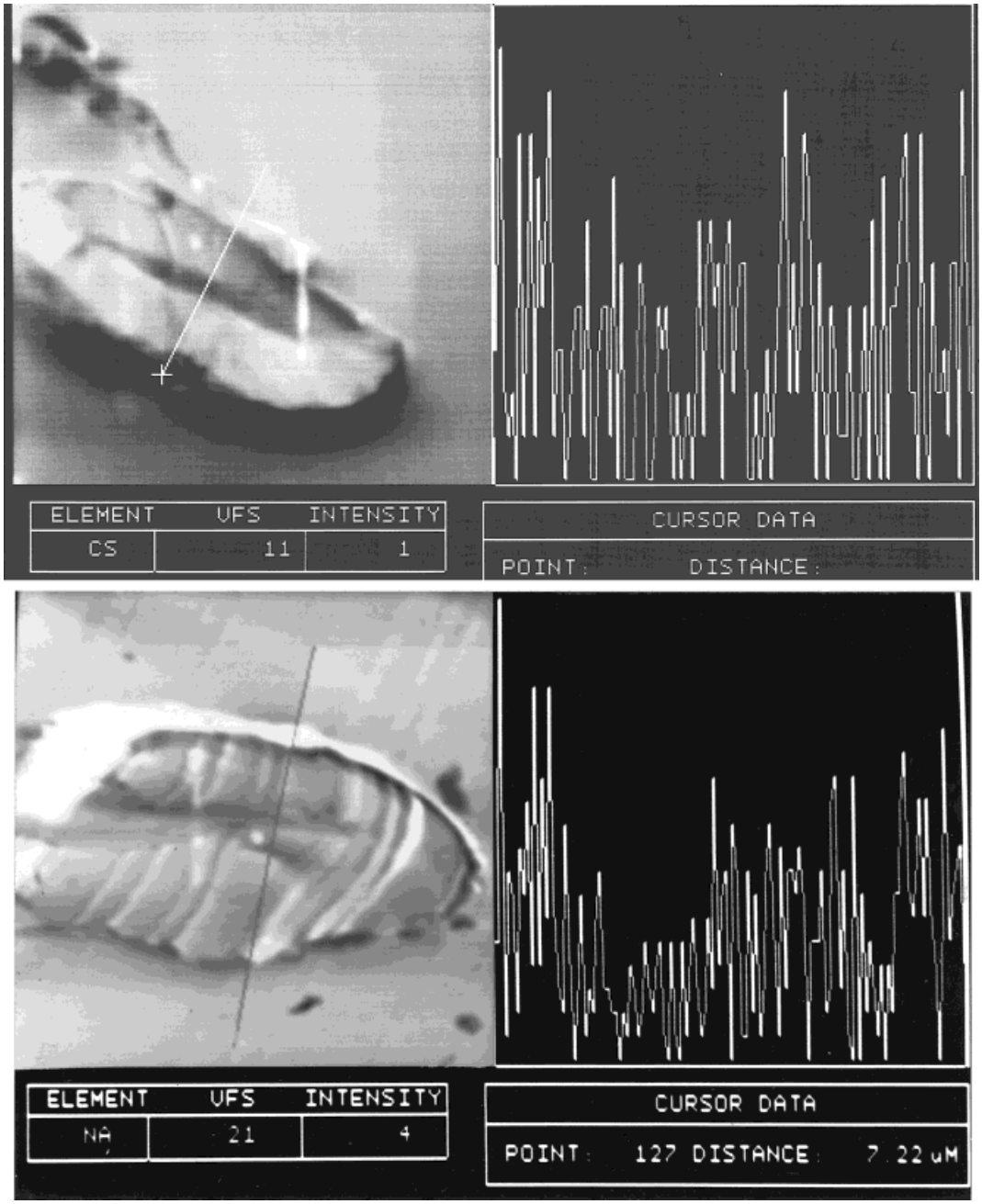

Figure 5 AEM analysis of control, ungrafted NSK fibers. Upper left: STEM image showing a cross section from a cesium ion exchanged fiber. The white line across this fiber denotes the electron beam path; 5000× original magnification. Upper right: a line scan for cesium, with the x axis denoting distance along the white line in the STEM image and the y axis denoting cesium X-ray counts, the full vertical scale being 11 counts. Lower left: STEM image showing a cross section from a hydrolyzed, washed fiber. The dark line across the fiber denotes the electron beam path; line scan length is 7.2 μm; 10,000× original magnification. Lower right: a line scan for sodium, the full vertical scale being 21 counts.

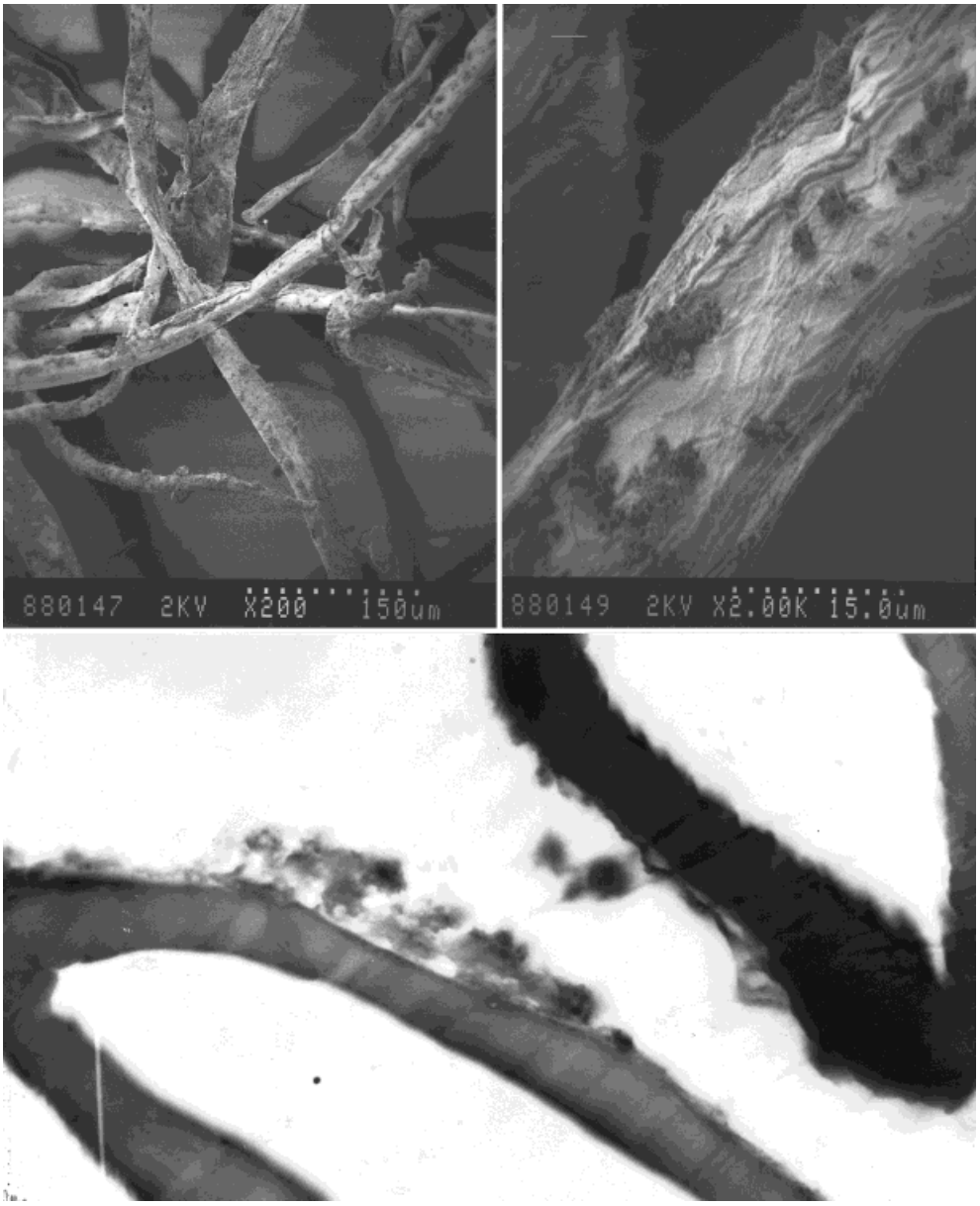

Figure 6 Unhydrolyzed acrylonitrile-grafted fibers. The fibers were grafted 2 : 1 polymer/fiber by weight. Upper left: SEM image, 200× original magnification. Upper right: Higher magnification SEM image; 2000× original magnification. Lower image: STEM micrograph of two plastic-embedded, cross-sectioned fibers; 5000× original magnification.

was dissolved in 1*N* HCl prepared with distilled deionized water and assayed for cesium using atomic absorption spectrophotometry.

Sodium Assay

Following the overnight washing, fibers were ashed and analyzed by atomic absorption spectrophotometry as described above for cesium.

Carboxylate Level Assay

Carboxylate levels in grafted fibers were measured by ^{13}C-NMR.[1]

Grafted Fiber Nitrogen Assay

The nitrogen content of unhydrolyzed acrylonitrile-grafted fibers was determined using the Carlo–Erba nitrogen analyzer.

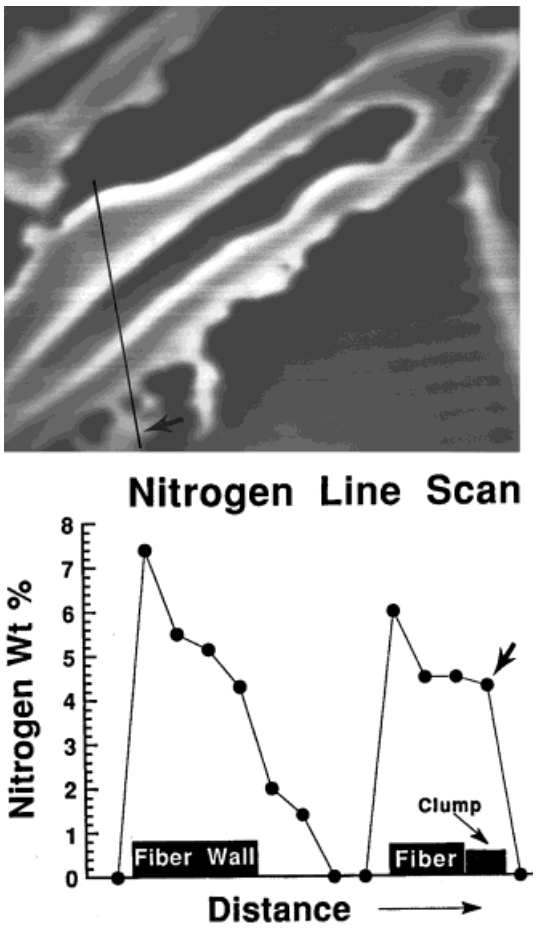

Figure 7 Upper image: STEM image from electron microprobe of a cross-sectioned, plastic-embedded unhydrolyzed acrylonitrile-grafted fiber. Dark line across the fiber walls denotes the path along which discrete points were analyzed for nitrogen. Black arrow points to pendant "fuzzy clumps"; 4000× original magnification. Lower image: Graph showing (semiquantitative) nitrogen levels versus distance along the black line in the STEM image. Location of fiber walls are denoted on the *x* axis, as is the fuzzy clump.

RESULTS AND DISCUSSION

Control Fibers

An SEM image of control, ungrafted NSK fibers is shown in Figure 1(a) and at higher magnification in Figure 1(b). The fibers are typically flattened and ribbonlike with a rough, fibrillar surface. The surface fibrils likely are remnants from the primary wall. A TEM image of an ultrathin, heavy metal stained ungrafted fiber is shown in Figure 2. Considerable ultrastructural detail is present; for instance, the collapsed fiber lumen and the differing orientation of the cellulose fibrils in the S1 and S2 layers are clearly visible. In contrast, a TEM image from a 1-μm thick section of an unstained ungrafted fiber wall is shown in Figure 3. The image has a grainy appearance in this thick section. The fiber wall is essentially featureless, not only because the section is unstained, but also because the thickness of the section exceeds the dimensions of the structural components within the fiber wall. This featureless appearance of the control fibers is in marked contrast to the appearance of grafted fibers, as will be shown subsequently. Similarly, an STEM image of an unstained 1-μm thick fiber cross section in Figure 4 reveals little ultrastructural detail. The collapsed fiber lumen is apparent and is similar to that in Figure 2. The outer surface of the fiber is darker (more dense) and occasionally has a frayed appearance. However, cross sections of the fiber wall, when not marred by linear knife marks incurred during sectioning, appear smooth and featureless.

AEM analysis of a control ungrafted fiber treated by method 1 is shown in the upper image of Figure 5. The upper left image is an STEM micrograph of a cross-sectioned fiber. The white dotted line superimposed on this image depicts the path scanned by the electron beam while monitoring the cesium X-ray signal. The right image is a display of the cesium X-ray intensity (*y* axis) versus the distance along the scanned line (*x* axis). The vertical scale maximum is only 11 counts, which is the "background" (noise) level. The cesium counts within the fiber wall are indistinguishable from those in the embedding plastic, further indicating that cesium is not detected within the control fiber. The lower image in Figure 5 is from a control ungrafted fiber that was hydrolyzed and treated by method 2. Because the vertical scale maximum for sodium is only 21 counts and fiber levels are indistinguishable from those in the embedding plastic, it can be concluded that sodium is not a constituent of the treated control fiber.

Unhydrolyzed Acrylonitrile-Grafted Fibers Dried from Solvent

Low and high magnification SEM images of unhydrolyzed acrylonitrile-grafted fibers are shown in the upper images of Figure 6. The fibers were grafted 2 : 1 polymer/fiber by weight. Compared with the ungrafted fibers (Fig. 1), acrylonitrile-

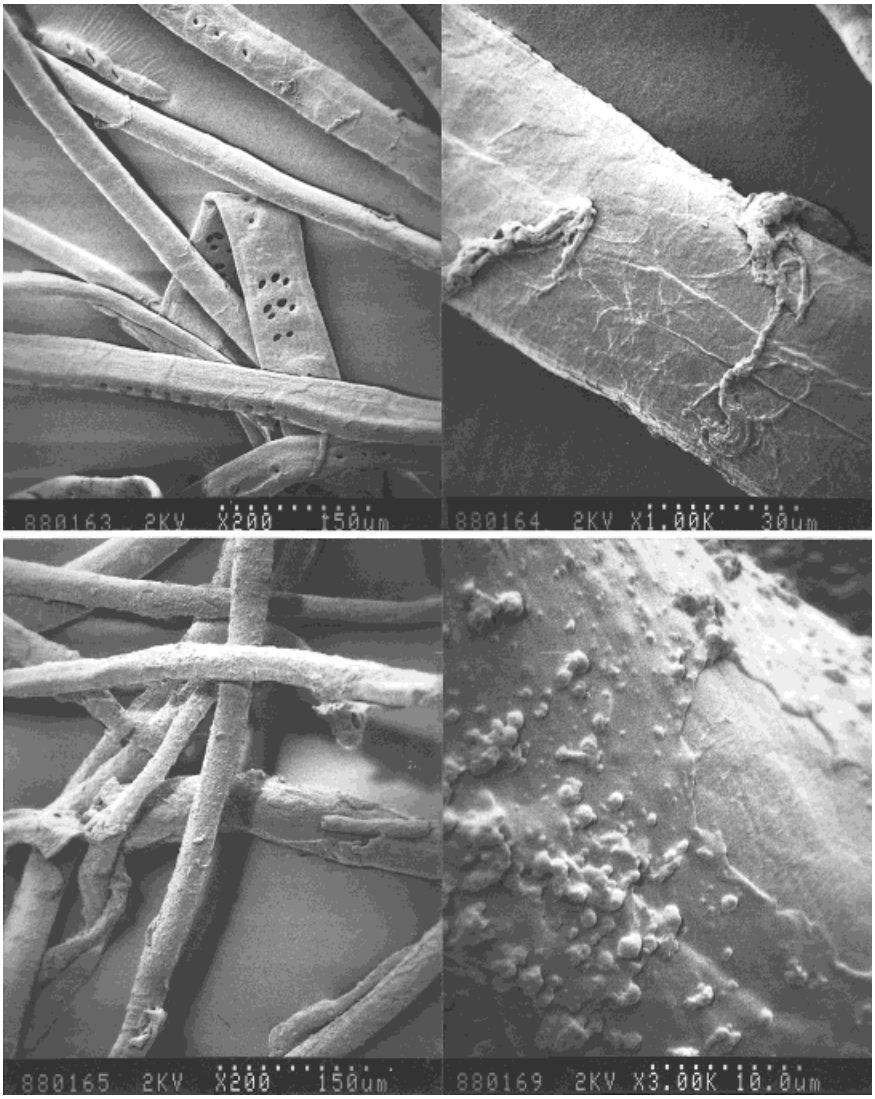

Figure 8 Unhydrolyzed methyl acrylate grafted fibers. Upper left: SEM image of fibers grafted 2 : 1 polymer/fiber by weight, 200× original magnification. Upper right: Higher magnification SEM image of 2 : 1 grafted fibers; 1000× original magnification. Lower left: SEM image of fibers grafted 4 : 1 polymer/fiber, 200× original magnification. Lower right: Higher magnification SEM image of 4 : 1 grafted fibers; 3000× original magnification.

grafted fibers are plumper. The surface is dotted with distinctive growths appearing as protruding clumps of tangled, tufted polymeric material. The unobscured surface also appears coated; the fine surface fibrils observed in control fibers are not evident, and surface features are less distinct. As seen in cross section in the lower STEM image, the fibers are swollen with an open lumen. The fiber wall in cross section is featureless and similar in appearance to the control fiber (Fig. 4). Clumps protruding from the fiber surface have the appearance of tangled, tufted, fuzzy threads.

Microprobe analysis of fiber cross sections is shown in Figure 7. The black arrow in the STEM image shows the path along which discrete points were selected for nitrogen (acrylonitrile) analysis. The graph below shows the measured (semiquantitative) nitrogen profiles across the two fiber

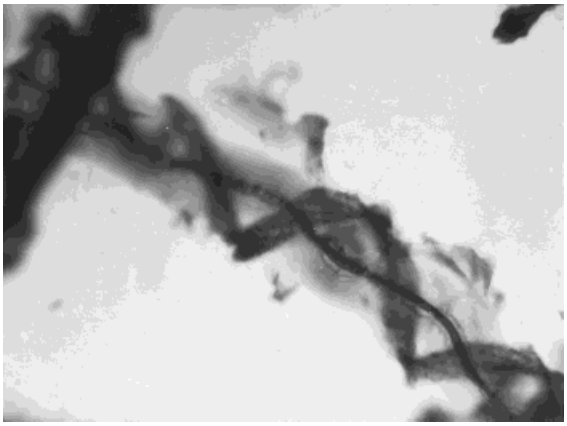

Figure 9 Light micrograph of hydrolyzed methyl acrylate grafted fiber in water; 80× original magnification.

walls, with the x axis corresponding to the distance along the analyzed path. The positions of the fiber walls are indicated on the x axis. Nitrogen (acrylonitrile) is present throughout the fiber, indicating a homogeneous distribution of the polymer. The analysis point indicated by an arrow in the STEM image, the corresponding point similarly located on the graph, was obtained from the fuzzy clump extending from the fiber surface. The fuzzy clump embedded in the plastic resin contains nitrogen in amounts approximately equivalent to the interior of the fiber. The y-axis nitrogen values shown in this figure are underestimated because the nitrogen X-ray counts from the thin section were compared with a bulk (infinitely thick) standard. The fibers actually contain about 14% nitrogen from bulk analysis.

Methyl Acrylate Grafted Fibers

Figure 8 shows low and high magnification SEM images of unhydrolyzed methyl acrylate grafted fibers dried from solvent. The upper images are from fibers grafted at a 2 : 1 ratio of polymer to fiber weight. The fibers have a surface coating of polymer; they have a smooth, nearly featureless appearance, although at higher magnification some surface detail is still evident. The lower images are from fibers grafted at a 4 : 1 ratio of polymer to fiber weight. The fibers are more rounded in appearance. The polymer coating is clearly thicker; the normal fiber surface structure is nearly completely concealed. At higher magnification the surface coating now has a textured, lumpy appearance.

The hydrolyzed grafted fiber in water has a swollen S2 layer and a disrupted S1 layer, as shown in the light micrograph of Figure 9. The S1 layer, or remnant thereof, remains associated with the fiber, often forming a spiral around the (lightly stained) swollen S2 layer. The darker staining core of this fiber is the S3 layer. With a disrupted S1 layer, the S2 layer is unrestrained and it swells, apparently to a natural limit.

Low and high magnification SEM images of hydrolyzed grafted fibers dried from ethanol are shown in Figure 10. As shown at higher magnification in Figure 10(b), the disrupted outer layer is characterized by visible, approximately circumferential microfibrils characteristic of the S1 layer whereas the underlying fiber is characterized by the more longitudinal microfibrils characteristic of the S2 layer.[27] As shown in Figure 10(a), the S1 layer is longitudinally ruptured and forms extended "wings" that continue to partially surround the rounded S2 layer. The rightmost fiber in Figure 10(a) shows a ruptured S1 layer that is spiraling around the S2 layer (arrows). The S2 layer is swollen and cylindrical with a ropelike appearance. The filamentous ropelike appearance of the surface of the S2 layer in Figure 10(a,b) is somewhat deceiving in that other images show the interior of the S2 layer to have a dual filament/lamellar structure similar to that described by Scallan.[28] In the tilted end-on view of a grafted fiber in Figure 10(c), the right side of the fiber has a lamellar appearance and different planes of separation and termination. Lamellae are particularly evident in the underlying lower right region of this fiber. However, lone fibrils are clearly seen protruding from the surface (black arrow); the very end of this fiber (white arrow), shown at higher magnification in Figure 10(d), appears to have a fibrillar, almost tubular substructure.

STEM images of unstained cross sections from these grafted, hydrolyzed fibers are shown in Figure 11. The upper image shows the wings of the ruptured S1 layer still joined to the S2 layer over a small area. The S2 layer appears swollen and considerably thicker than that of the control and appears to have a mottled substructure that was not apparent in ungrafted fibers (Fig. 4). As shown in the lower image obtained at higher magnification from a different fiber, the S2 layer appears to contain holes or microvoids, which are particularly prominent in the upper left corner

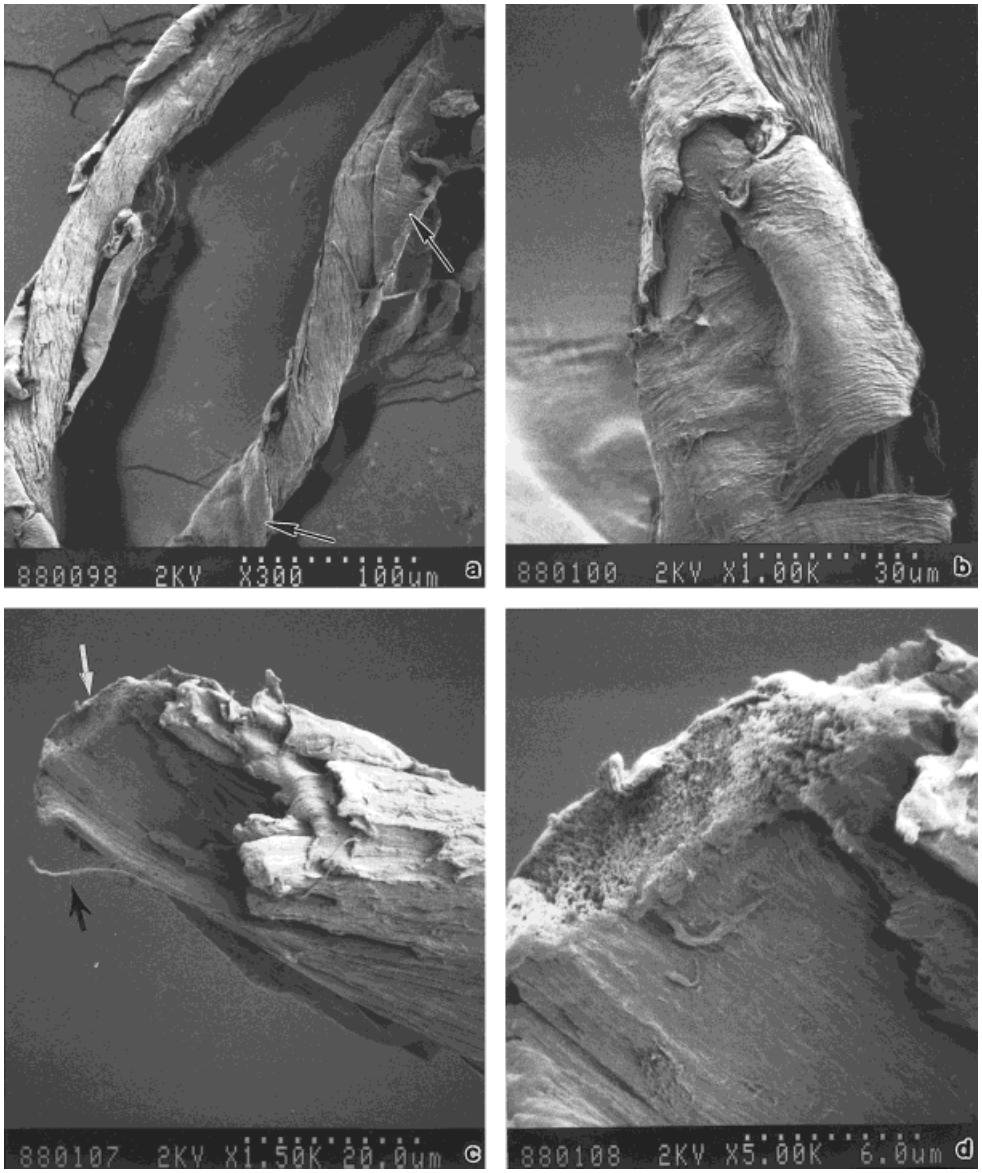

Figure 10 Hydrolyzed methyl acrylate grafted fibers, grafted 3 : 1 polymer/fiber by weight, dried from ethanol. (a) SEM image of two fibers; 300× original magnification; (b) Higher magnification SEM image; 1000× original magnification; (c) SEM image of broken fiber end; 150× original magnification. Black arrow points to fibril protruding from surface; others are visible. (d) Higher magnification (5000× original magnification) SEM image from region denoted by white arrow in (c).

(arrow). Very occasionally large "pores" are present within the S2 layer, two of which are shown in the middle of this image.

TEM images of unstained cross sections from grafted hydrolyzed fibers are shown in Figure 12. Figure 12(a) shows a low magnification view of the S2 layer. A diversity of substructure is apparent in this layer, suggesting a coexistence of "lamellar" and "filamentous" regions. This striking substructure is in marked contrast to the featureless appearance of ungrafted fibers in thick sections (Fig. 3). In Figure 12(b) the S2 wall appears to consist of interwoven light and dark domains coexisting with holes or microvoids that are seen

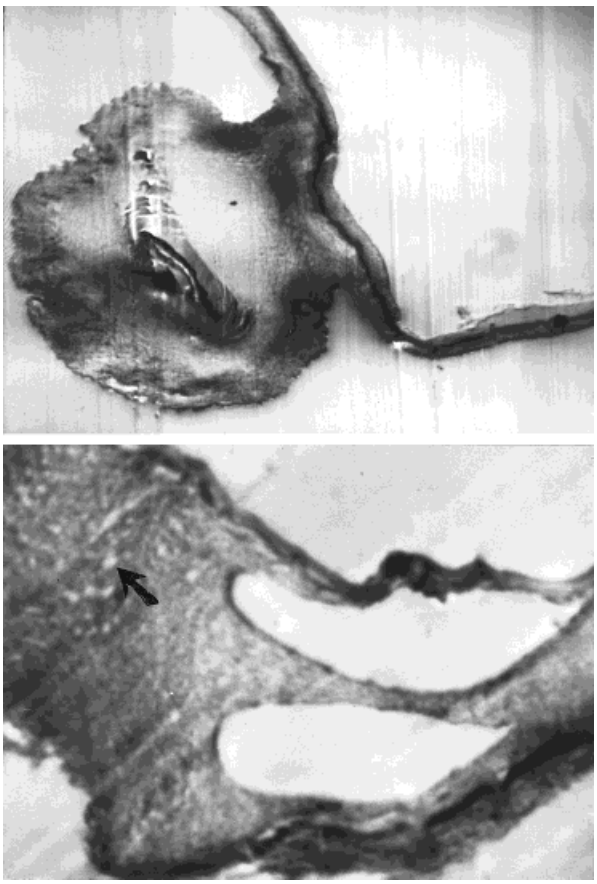

Figure 11 STEM images of hydrolyzed methyl acrylate grafted fibers, 3 : 1 polymer/fiber by weight, dried from ethanol. Upper image: Cross-sectioned plastic-embedded fiber showing S1 "wings" and S2 substructure; 2000× original magnification. Lower image: Higher magnification of cross-sectioned plastic-embedded fiber wall showing large "pores" in the S2 wall (middle of image) as well as microvoids, particularly evident in the left side of the image (arrow). The clear expanse in the upper part of this image is the fiber lumen; 10,000× original magnification.

as bright and approximately circular features in this image (arrow). The microvoids are similar to those seen in the lower image of Figure 11. The microvoids average about 0.1 μm in diameter, nearly 2 orders of magnitude larger than voids in solvent-dried ungrafted fibers and an order of magnitude larger than the pores created by beating.[5–7] In Figure 12(c) a "spotted" architecture is observed, which we interpret as separate islands of polymer in the cellulose matrix. This spotted architecture is primarily observed toward the fiber outer wall; as the periphery is approached, the dark spots become larger and more irregular. In Figure 12(d) an apparently ordered lamellar structure is observed that has a lamellar spacing of about 0.05 μm.

The marked changes in S2 wall morphology would strongly suggest that methyl acrylate grafting has occurred throughout the fiber wall, similar to the results with acrylonitrile grafting (Fig. 7). To determine the methyl acrylate distribution in the fiber walls more directly, AEM was used to localize Cs and Na counterion tags of the acrylate carboxylate groups. The ability of these cations to tag carboxylate groups is shown in Figure 13. Cesium ion exchange (method 1) accurately labels carboxylate groups and is shown in the upper graph of Figure 13. Cesium levels measured by atomic absorption spectrophotometry (y axis) accurately reflect the predicted cesium concentration (x axis) based on the fiber carboxylate number measured by ^{13}C-NMR. Similarly, the lower graph shows that sodium is directly correlated with carboxylate levels and, by extrapolation of the linear regression line to the origin, that residual uncomplexed sodium is small. The cerium used in polymer grafting was not detected in hydrolyzed fibers by AEM and thus is either not present or below the AEM detection limit ($\sim$ 0.2 wt %); consequently, it does not interfere with the Cs or Na tagging.

A relatively homogeneous distribution of methyl acrylate throughout the wood fiber was demonstrated by AEM using cesium or sodium as markers of the carboxylate functionality. Figure 14(a,b) shows STEM images on the left and line scans on the right. Figure 14(a) shows a fiber grafted 1 : 1 with acrylate and prepared by method 1. The associated line scan shows an enhancement of acrylate (cesium) at the fiber surface, an approximately uniform distribution across the remaining fiber wall and S3 layer, and the expected lack of cesium as the fiber lumen is traversed. Figure 14(b) shows a fiber grafted 3 : 1 with methyl acrylate and prepared by method 2. In contrast to the enhancement of grafting at the fiber outer wall shown in Figure 14(a), the line scan of Figure 14(b) exhibits a relatively uniform methyl acrylate (sodium) level throughout the fiber, including the S1, S2, and S3 layers. Figure 14(c) shows an STEM image on the left and the corresponding X-ray map for sodium on the right. White denotes high sodium (acrylate) levels, and the two images correspond point by point.

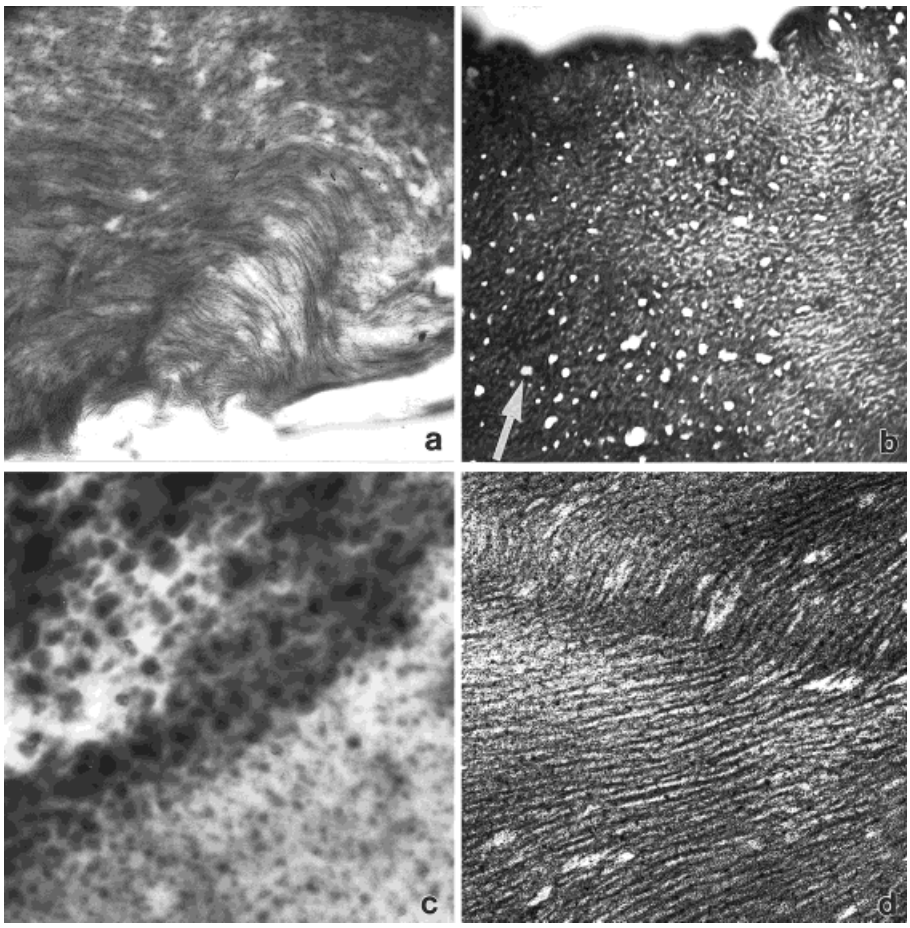

Figure 12 TEM micrographs of 1-μm thick hydrolyzed methyl acrylate grafted fibers, 3 : 1 polymer/fiber, dried from ethanol. (a) Low magnification image showing the coexistence of lamellar and filamentous substructure in the S2 wall; 3500× original magnification. (b) S2 wall showing the coexistence of microvoids (e.g., white arrow) and filamentous "woven" light and dark domains; 12,000× original magnification. (c) S1/S2 wall showing a "spotted" substructure. The S1 layer periphery is toward the upper left corner of this image; 7000× original magnification. (d) S2 wall showing a periodic lamellar pattern; 20,000× original magnification.

As shown for this fiber that was grafted 3 : 1 and prepared by method 2, acrylate levels were high both at the outer fiber surface and in the S3 layer. In general, grafting levels were uniform across the fiber wall or enhanced at the outer or occasionally inner periphery. Surface enhancement of grafts did not appear to be a function of grafting levels. Grafting was never localized only at the fiber surface.

CONCLUSIONS

Softwood Kraft fibers were grafted with acrylate or acrylonitrile as described in the preceding article. This grafting process dramatically increased the rate and capacity for water absorption. To better understand the structural basis for the alterations in water uptake, we investigated the localization of polymer grafts throughout the cellulose fiber and the alterations of fiber morphology induced by the grafting process.

SEM analysis showed that polymer was present on the cellulose fiber surface following methyl acrylate grafting, and following acrylonitrile grafting it was present on the fiber surface and extended outward from the surface in the form of tangled tufts of polymer. AEM studies showed

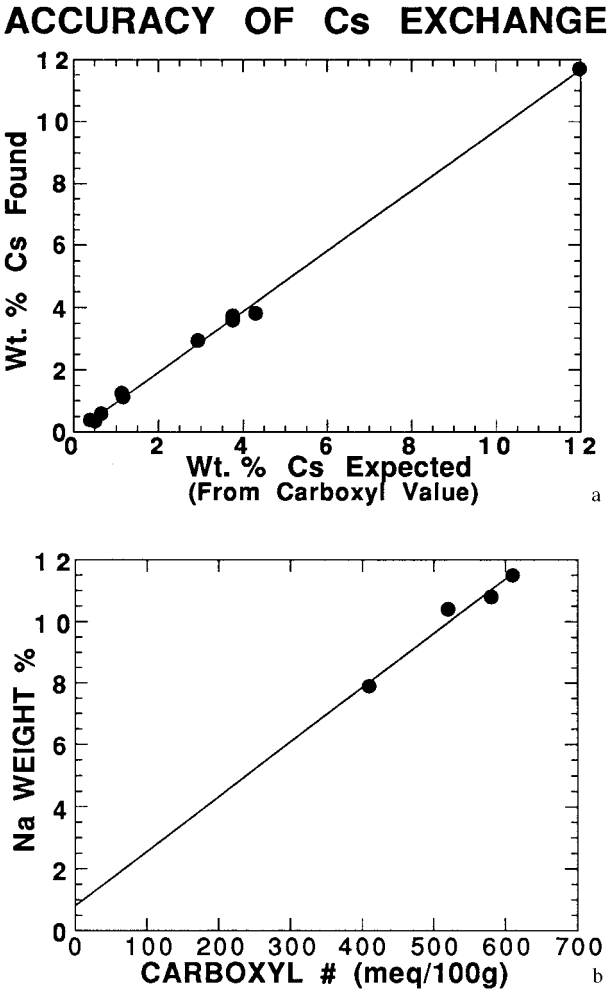

Figure 13 (a) Demonstration that cesium ion exchange accurately accounts for total fiber carboxylate groups. Measured cesium (atomic absorption spectrometry measurement) on the *y* axis is graphed versus the predicted cesium amount based on the carboxyl number of grafted fibers. (b) Demonstration that (hydrolyzed) fiber sodium remaining after extensive washing is proportional to the carboxylate number. Extrapolation of the data points to the origin indicates that very little "uncomplexed" sodium is present in these fibers (<10%).

with both polymers that grafting occurred extensively throughout the cellulose wall. Often grafting levels were enhanced near the fiber periphery and occasionally were enhanced in the S3 layer.

Our TEM observations on the somewhat confusing interplay of fibrillar and lamellar structures in the interior of the S2 wall of hydrolyzed acrylate-grafted fibers dried from solvent are very similar to previous light microscope (LM) observations made on alkali-swollen fibers.[29] In those LM studies, the secondary wall could be disrupted into a variety of forms (layers, lamellae, fibrils, spherical units) similar to the structures we observed. This diversity of form was ascribed to "planes of structural weakness" among anastomosing, threadlike structures of cellulose.[29] The anastomosing fibrils were held together by branching and lateral interconnections, giving rise to many diverse and complex structural patterns, including lamellae "somewhat less than 0.1 μm,"[29] similar to the pattern we observe (Fig. 12). The intrinsic ability of cellulose to form lamellar structures was described previously.[30]

We believe that the enhanced capacity and rate of water uptake observed in these fibers[1] can be explained by three changes in the cellulose fiber wall that were induced by the grafting process. First, disruption of the S1 layer removes the constraints on S2 layer swelling. The approximately circumferential S1 layer that normally serves to restrain fiber imbibition and swelling[31] is torn essentially longitudinally over the fiber length (likely during hydrolysis), freeing the S2 layer and allowing it to expand to its capacity. Second, chemical alterations in the composition of the S2 layer provide a strong osmotic force for water uptake. The addition of high levels of sodium ions within the fiber wall provides an extremely strong force for water uptake that is likely responsible for the S1 wall rupture. Third, alterations in the structure of the S2 layer enhance capillarity and provide the capacity for rapid and extensive swelling. We believe grafting occurred throughout amorphous regions of swollen cellulose. Due to the interconnecting polymer domains, the grafted fiber remains locked in a relatively expanded configuration following dehydration. Shrinkage that does occur during dehydration produces a system of voids, including stretched pore structures. The resulting combination, consisting of polymer conduits, an enhanced presence of void structures, and the existence of large pores, provides a large increase in capillarity. The enhanced absorptive capacity and rate of water uptake is thus due to enhanced capillarity acting in concert with a strong osmotic pressure to quickly attract, distribute, and retain water in the pores and polymer domains of the grafted fibers.

AEM is a useful technique for investigating the distribution of polymer grafts in cellulose fibers. Unlike TEM techniques used previously, AEM does not rely on differential solubilities and disso-

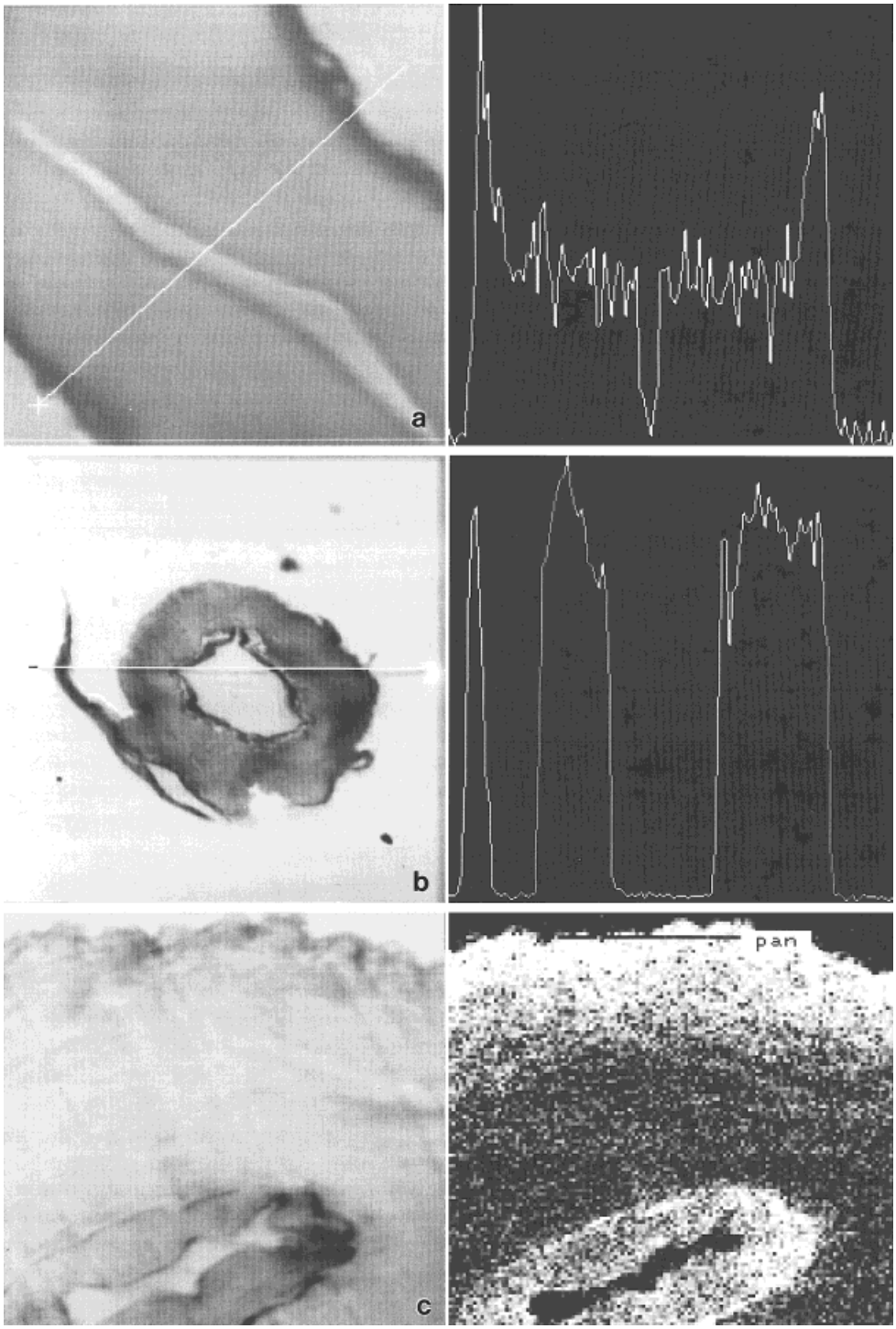

Figure 14 AEM of methyl acrylate grafted fibers dried from ethanol. (a) Cesium line profile across a fiber grafted 1 : 1. STEM image on left (15,000× original magnification), cesium profile on right showing approximately twofold surface enhancement of carboxylate (cesium) at the fiber surface, but nevertheless a substantial amount of cesium throughout the S2 wall. Surface enhancement of the S3 layer is not observed. The vertical scale is 100 counts. (b) Sodium line profile across a fiber grafted 3 : 1. STEM image on left (3000× original magnification), sodium profile on right showing a uniform distribution of carboxylate groups across the S1, S2, and S3 layers. The vertical scale is 2900 counts. (c) Sodium X-ray map of a fiber grafted 3 : 1. STEM image on left (10,000× original magnification), corresponding X-ray map on right. White in the X-ray map denotes high sodium levels. Carboxylate levels (sodium) are enhanced at the fiber periphery and S3 layer.

lution and washing techniques to visualize polymer distributions. Resolution in the STEM mode is good, revealing submicron structure. Sample preparation can be anhydrous, avoiding swelling artifacts. In the case of polymers containing intrinsically unique elements like nitrogen, polymer localization can be directly determined. In the case of polymers with distinguishing functional groups such as carboxylates, the use of inorganic counterions can provide polymer localization with minimal sample preparation. Although we used microprobe analysis for nitrogen measurements, analytical electron microscopes fitted with thin EDS detector windows have the capacity to directly measure nitrogen. Finally, an additional advantage of AEM is that results in the form of X-ray counts are directly quantifiable. Although not done in this study, full quantitation is readily obtained (with appropriate standards) using the Hall technique.[32] As illustrated in the line scans of Figure 14, qualitative results are obtained automatically.

REFERENCES

1. E. Rezai and R. R. Warner, *J. Appl. Polym. Sci.,* **65,** 1463 (1997).
2. A. M. Schwartz, in *Chemistry and Physics of Interfaces—II,* D. E. Gushee, Ed., American Chemical Society Publications, Washington, D.C., 1971, p. 1.
3. A. J. Panshin and C. de Zeeuw, Eds., *Textbook of Wood Technology,* 4th ed., McGraw–Hill, New York, 1980, p. 95.
4. A. J. Stamm, *Wood and Cellulose Science,* Ronald Press Co., New York, 1964, p. 145.
5. J. E. Stone and A. M. Scallan, *J. Polym. Sci., C,* **11,** 13 (1965).
6. T. Lindstrom, in *Paper: Structure and Properties,* J. A. Bristow and P. Kolseth, Eds., Marcel Dekker, New York, 1986, p. 99.
7. D. H. Page and J. H. de Grace, *Tappi,* **50,** 489 (1967).
8. R. Barbucci, M. Casolaro, A. Magnani, C. Roncolini, and P. Ferruti, *Polymer,* **30,** 1754 (1989).
9. W. R. Goynes and J. A. Harris, *J. Polym. Sci., C,* **37,** 277 (1972).
10. J. T. Guthrie and P. D. Tune, *J. Polym. Sci. Part A: Polym. Chem.,* **29,** 1301 (1991).
11. P. F. LePoutre, H. B. Hopfenberg, and V. Stannett, *J. Polym. Sci., C,* **37,** 309 (1972).
12. S. N. Bhattacharyya and D. Maldas, *J. Appl. Polym. Sci.,* **29,** 1559 (1984).
13. A. Basak, P. L. Nayak, and S. Lenka, *J. Appl. Polym. Sci.,* **41,** 311 (1990).
14. S. Kaizerman, G. Mino, and L. F. Meinhold, *Textile Res. J.,* **32,** 136 (1962).
15. Y. Iwakura, T. Kurosaki, K. Uno, and Y. Imai, *J. Polym. Sci., C,* **4,** 673 (1964).
16. R. M. Reinhardt, J. D. Reid, and G. C. Daul, *Textile Res. J.,* **26,** 1 (1956).
17. J. C. Arthur, Jr. and R. J. Demint, *Textile Res. J.,* **30,** 505 (1960).
18. M. L. Rollins, A. M. Cannizzaro, F. A. Blouin, and J. C. Arthur, Jr., *J. Appl. Polym. Sci.,* **12,** 71 (1968).
19. J. A. Harris, J. C. Arthur, Jr., and J. H. Carra, *J. Appl. Polym. Sci.,* **22,** 905 (1978).
20. A. Hebeish and J. T. Guthrie, *The Chemistry and Technology of Cellulosic Copolymers,* Springer–Verlag, New York, 1981, p. 245.
21. K. Kaji, *J. Appl. Polym. Sci.,* **32,** 4405 (1986).
22. H. Kubota and Y. Hata, *J. Appl. Polym. Sci.,* **41,** 689 (1990).
23. M. Rigdahl, B. Westerlind, H. Hollmark, and A. de Ruvo, *J. Polym. Sci., Polym. Lett. Ed.,* **21,** 205 (1983).
24. J. A. Harris, J. C. Arthur, Jr., and W. R. Goynes, Jr., *J. Appl. Polym. Sci.,* **24,** 201 (1979).
25. J. D. Timpa, L. H. Chance, and W. R. Goynes, Jr., *Dyestuff Reporter,* **68,** 60 (1979).
26. M. A. Hyatt, *Principles and Techniques of Electron Microscopy,* Vol. 1, Van Nostrand Reinhold, New York, 1970.
27. E. Sjostrom, *Wood Chemistry: Fundamentals and Applications,* Academic Press, New York, 1981, p. 16.
28. A. M. Scallan, *Wood Sci.,* **6,** 266 (1974).
29. I. W. Bailey, *Ind. Eng. Chem.,* **30,** 40 (1938).
30. J. Giasson, J.-F. Revol, A. M. Ritcey, and D. G. Gray, *Biopolymers,* **27,** 1999 (1988).
31. A. J. Stamm, *Wood and Cellulose Science,* Ronald Press Co., New York, 1964, p. 22.
32. T. A. Hall, in *Physical Techniques in Biological Research,* Vol. 1A, G. Oster, Ed., Academic Press, New York, 1971, p. 157.